CHEMPHYSCHEM

DOI: 10.1002/cphc.200800596

Direct Visualization of the Chemical Mechanism in SERRS of 4-Aminothiophenol/Metal Complexes and Metal/4-Aminothiophenol/Metal Junctions**

Mengtao Sun*[a] and Hongxing Xu[a, b]

We theoretically investigate the mechanism of chemical enhancement of surface-enhanced resonance Raman scattering (SERRS) of para*-aminothiophenol (PATP)/metal complexes and metal/PATP/metal junctions. The method of charge difference density is used to visualize intracluster excitation and charge transfer (CT) between PATP and metal during the process of resonant electronic transitions. It is found that the selective enhancement of the b_2 mode in SERRS spectra result not only from Albrecht's A term (the Frank–Condon term), but also from the Herzberg–Teller term (Albrecht's B mechanism) via resonant CT. For the metal/PATP/metal junctions, the calculated results reveal that the Raman spectrum is of SERRS nature and the nontotally symmetric b_2 mode is strongly enhanced at the incident wavelength of 1064 nm when Au and Ag nanoparticles are the first and second layer, respectively, and the dominant enhancement mechanism is the Herzberg–Teller term in chemical enhancement via tunneling charge transfer (intervalence electron transfer from the Ag cluster to the Au cluster). When the first and second layers were inverted (i.e. the Ag and Au nanoparticles are the first and second layers, respectively), the Raman spectrum at an incident wavelength of 1064 nm is due to normal Raman scattering, and the nontotally symmetric b_2 mode is not strongly enhanced. Our theoretical results not only support the experimental findings, but also provide a clear physical interpretation.*

1. Introduction

Surface-enhanced Raman scattering (SERS)[1–6] was discovered about thirty years ago. There is general agreement that SERS occurs by electromagnetic enhancement (EM) and chemical enhancement mechanisms.[7–14] The former is caused by local surface plasmon polaritons,[7–8] which usually enhance the Raman spectrum over a large frequency range, and the latter is due to changes in the electronic structure of molecule adsorbed on metal surfaces, whereby some Raman peaks undergo enormous selective enhancement.[9–14] Chemical enhancement is typically explained by the charge-transfer (CT) mechanism.

When a molecule is adsorbed on a metal surface, new electronic states are formed due to chemisorption. The new electronic states may serve as resonant intermediate states in Raman scattering. If the Fermi level of the metal is located between the HOMO and the LUMO in energy, CT excitations may likely occur at lower energy than intrinsic intramolecular excitations of the adsorbate.[15,16] According to Albrecht's notation,[10a] in the CT mechanism via Albrecht's A term (Frank–Condon term) only the totally symmetric modes are resonantly enhanced when the laser excitation is close to an allowed electronic transition, and only one excited state is involved. The resonance Raman effects for vibrational modes that are nontotally symmetric, such as b_2, are usually observed when the b_2 modes couple two excited states of the chromophore. The product of the symmetry of both excited states should be equal or contain the b_2 symmetry. This mechanism is known as the Herzberg–Teller mechanism or B mechanism in Albrecht's notation.

Recently, we developed a novel method of charge difference density to visualize intracluster (electron and hole are localized on metal cluster) excitation and CT (CT between molecule and metal cluster) excitations for the case of pyridine adsorbed on Ag nanoparticles.[13,14] Intracluster excitation and CT excitation are direct evidence for the EM mechanism and the chemical mechanism, respectively.

The SERS of *para*-aminothiophenol (PATP) adsorbed on different metal surfaces has been extensively studied experimentally.[17–28] Recently, more and more effort has been devoted to studying the properties of metal/molecule/metal sandwich architectures,[19,23–25,28] and typically silver and gold nanoparticles were interconnected by PATP. Strong a_1 and b_2 modes dominate the SERS spectra when molecules are attached in metal complexes and when they are located in the junction of metal/molecule/metal structures. These selective enhancements of b_2 modes are ascribed to the effect of chemical enhancement.

[a] *Prof. Dr. M. Sun, Prof. Dr. H. Xu*
Beijing National Laboratory for Condensed Matter Physics and
Laboratory of Soft Matter Physics, Institute of Physics
Chinese Academy of Sciences
P. O. Box 603-146, Beijing, 100190 (P. R. China)
Fax: (+86) 10-82649228
E-mail: mtsun@aphy.iphy.ac.cn

[b] *Prof. Dr. H. Xu*
Division of Solid State Physics
Lund University, Lund 22100 (Sweden)

[**] *SERRS: Surface-enhanced resonance Raman scattering.*

Supporting information for this article is available on the WWW under http://dx.doi.org/10.1002/cphc.200800596.

Herein, using the visual method of charge difference density, we theoretically investigate when and how CT excitations happen and the mechanism by which CT selectively enhances b_2 modes of PATP in metal complexes of molecules and in metal/molecule/metal junctions (here metal = Au or Ag clusters). We focus on 1) the role of chemical mechanism in SERS of PATP at incident wavelengths of 514.4 and 632.8 nm for PATP/Ag_5 and PATP/Au_5 complexes, respectively; and 2) the role of the chemical mechanism in SERS of PATP at an incident wavelength of 1064 nm when PATP chemically connects two metal clusters in a metal/PATP/metal junction model.

Methods

The optimized geometry and normal Raman spectrum of PATP (see Figure 1 a) in the ground state were obtained with density-functional theory (DFT),[29] B3LYP functional,[30,31] and 6-31G(d) basis set.

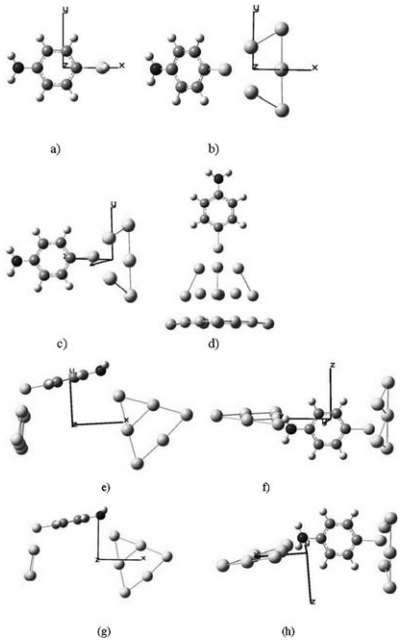

Figure 1. Theoretical geometries for a) PATP, b) PATP/Ag_5, c) PATP/Au_5, and d) PATP/Ag_5 complexes; e) Au_5/PATP/Ag_6 junction; f) side view of e); g) Ag_5/PATP/Ag_6 junction; and h) side view of g). Cartesian coordinates are shown.

The appearance of the 213 cm^{-1} band (assignable to Ag–S stretching[32] in the SERS spectrum) indicates that PATP is adsorbed onto the silver surface through the sulfur atom by rupture of the S–H bond in metal PATP complexes. PATP/Ag_5 and PATP/Au_5 models (see Figure 1 b and c) were used for simulating PATP adsorbed on silver and gold nanoparticles, respectively. As models of the metal/PATP/metal junctions studied experimentally in ref. [24], Au_5/PATP/Ag_6 (Figure 1 e and f) and Ag_5/PATP/Au_6 (Figure 1 g and h) junctions were adopted, in which Au_5 and Ag_5 clusters are bonded to the S atom of PATP, respectively (the Au and Ag nanoparticles form the first layer in the two above models for ref. [24], respectively). The absorption and SERS spectrum of metal/PATP/metal junctions were also investigated theoretically to interpret the experimental results in ref. [24].

Geometry optimization and frequency analysis of metal/PATP complexes and metal/PATP/metal junctions in the ground state were performed with DFT,[30] B3LYP functional,[31,32] and LanL2DZ basis set.[33] All models were fully optimized and there was no imaginary frequency. The optimized geometries of metal/PATP/metal junctions in the ground state are reported in the Supporting Information. Their normal Raman scattering (NRS) spectra were calculated with the same functional and basis set at the optimized ground-state geometry. Their absorption transition energies and oscillator strengths in absorption were calculated with time-dependent DFT (TDDFT),[34] B3LYP functional, and LanL2DZ basis set. The SERRS of the PATP/Au_5 complex was calculated with DFT, B3LYP functional, and LanL2DZ basis set at an incident wavelength of 632.8 nm. To study the effect of cluster size, the NRS spectrum and optical absorption spectrum of PATP/Ag_{19} complex were also calculated (the optimized geometry for the ground state is reported in the Supporting Information).[35] In order to compare and contrast the results of neutral PATP/Ag^{I}_5 and anionic PATP/Ag^{0}_5 complexes, the NRS spectra of anionic PATP/Ag^{0}_5 were calculated. To study the effect of the functional on the calculations, the B3PW91 functional was employed in the calculations of the ground- and excited-state properties in metal/PATP/metal junctions. All quantum chemical calculations were done with the Gaussian 03 suite.[36]

Absolute Raman intensities can be calculated as the differential Raman scattering cross section. For Stokes scattering with an experimental setup of 90° scattering angle and perpendicular plane-polarized light, the cross section is written as Equation (1)[37]

$$\frac{d\sigma}{d\Omega} = \frac{\pi^2}{\varepsilon_0^2}(\omega_{in} - \omega_p)^4 \frac{h}{8\pi^2 c\omega_p} S_p \frac{1}{45\left[1 - \exp(-hc\omega_p/k_B T)\right]} \quad (1)$$

where ω_{in} and ω_p are the frequency of the incident light and of the pth vibrational mode, respectively, and S_p is the Raman scattering factor (or Raman activity in units of $A^4 amu^{-1}$) [Eq. (2)]

$$S_p = 45\left(\frac{\partial\alpha_p}{\partial Q_p}\right)^2 + 7\left(\frac{\delta\gamma_p}{\partial Q_p}\right)^2 \quad (2)$$

which is a pure molecular property and independent of experimental setup. α_p and γ_p are the isotropic and anisotropic polarizabilities. For the normal Raman and Resonance spectra, we set $\omega_{in} =$ 0 nm and $\omega_{in} =$ 633 nm in Equation (1) in our calculations, respectively. In this paper, S_p were directly calculated with the Gaussian 03 suite.[36] The scale factor of the frequencies was set to 0.96 in our calculations[38] for comparison with experiment results.

The orientation of CT for the electronic resonance transitions were visualized by means of the charge difference density.[13,14]

2. Results and Discussion

2.1. Ground-State Properties and NRS Spectra for Metal/PATP Complexes and Metal/PATP/Metal Junctions

Due to the interaction between metal and molecule, static CT between metal and molecule occurs. For the PATP/Ag_5 complex, the static CT is 0.07 from Ag_5 cluster to PATP, while for the PATP/Au_5 complex the static CT is 0.21 from PATP to Au_5 cluster. The interaction strength between PATP and Au_5 cluster is much stronger than that between PATP and Ag_5 cluster, due to the larger amount of charge transfer between metal and molecule in the former. The CT between metal and molecule in the ground state results in an increase in static polarizabilities, which are listed in Table 1. The static charge redistribution

Table 1. Calculated static polarizabilities [a.u.] in the ground state for PATP, PATP/Ag_5 complex PATP/Au_5 complex, Au_5/PATP/Ag_6 junction, and Ag_5/PATP/Au_6 junction. Their Cartesian coordinates are shown in Figure 1.

	xx	*yy*	*zz*
PATP	130.653	77.567	42.848
PATP/Ag_5 complex	389.049	371.086	198.589
PATP/Au_5 complex	399.103	330.014	183.364
Au_5/PATP/Ag_6 junction	716.274	618.388	456.426
Ag_5/PATP/Au_6 junction	645.412	568.304	476.706

for the Au_5/PATP/Ag_6 and Ag_5/PATP/Au_6 junctions in the ground state is shown in Figure 2. For the Au_5/PATP/Ag_6 junction, the electrons transfer from PATP to the Au_5 and Ag_6 clusters, while for the Ag_5/PATP/Au_6 junction, the electrons transfer from PATP and Au_5 cluster to Ag_6 cluster. The calculated static polarizabilities of metal/PATP/metal junctions are also listed in Table 1.

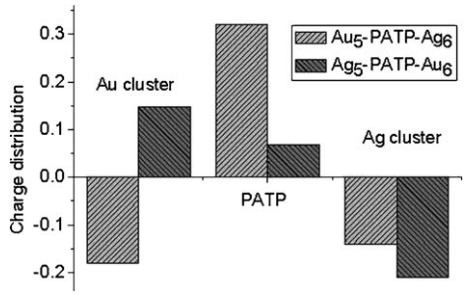

Figure 2. Charge redistribution for the Au_5/PATP/Ag_6 and Ag_5/PATP/Au_6 junctions in the ground state.

The calculated NRS spectra of PATP, PATP/Ag_5 complex, PATP/Au_5 complex, Au_5/PATP/Ag_6 junction, and Ag_5/PATP/Au_6 junction are shown in Figure 3. Due to the increased static polarizabilities of PATP/metal compared to isolated PATP, the two totally symmetric modes of the S–C and C=C bonds (see inset in Figure 3b) are strongly enhanced, by factors of about 30 and 50, respectively. Because the amount of CT between PATP and the Au_5 cluster is larger than that between PATP and the Ag_5 cluster, the enhancements for these two normal modes of the PATP/Au_5 complex (Figure 3e) are stronger than those of the PATP/Ag_5 complex (Figure 3b).

To study the influence of cluster size on the NRS spectrum, the NRS of PATP/Ag_{19} complex was calculated (see Figure 3c), and little influence of cluster size on the NRS profile was found. In order to compare the results for neutral PATP/Ag^{I}_5 and anionic PATP/Ag^{0}_5 complex, the NRS spectra of the anionic complex PATP/Ag^{0}_5 were calculated (see Figure 3d). Little difference in profile was found between the spectra for the neutral and anionic species, but the intensity of the latter is decreased.

The calculated NRS spectra of the Au_5/PATP/Ag_6 and Ag_5/PATP/Au_6 junctions are shown in Figure 3f and g, respectively. Minor differences in profile are found between the NRS spectra of Au_5/PATP/Ag_6 junction (and Ag_5/PATP/Au_6 junction) and the NRS spectra of PATP/Au_5 complex (and PATP/Ag_5 complex).

2.2. Optical Absorption Properties and SERRS Spectra for Metal/PATP Complexes

The calculated optical absorption spectra of the PATP/Ag_5 complex, PATP/Au_5 complex, and Au_5/PATP/Ag_6 junction are shown in Figure 4. For the PATP/Ag_5 complex, the second excited state (ca. 510 nm) is an optically allowed strong absorption peak, and this excited state is a CT excited state (see charge difference density in the inset), so the experimental SERRS spectra at an incident wavelength of 514.4 nm should be strongly enhanced by chemical enhancement via CT from PATP to the Ag_5 cluster. For the PATP/Au_5 complex, the first excited state (ca. 650 nm) has low oscillator strength, and this excited state is a CT excited state (see charge difference density in the inset), so the experimental SERRS spectra at an incident wavelength of 632.8 nm should be strongly enhanced by chemical enhancement due to CT from PATP to Au_5 cluster.

According to Albrecht's notation,[10a] in the enhancement via the Frank–Condon term only the totally symmetric modes are resonantly enhanced when the laser excitation is close to an allowed electronic transition, and only one excited state is involved. The resonance Raman effects for vibrational modes that are nontotally symmetric, such as b_2, are usually observed when the b_2 modes couple two excited states of the chromophore. The product of the symmetry of both excited states should be equal to or contain the b_2 symmetry. This mechanism is known as the Herzberg–Teller mechanism.

From Figure 4a and b, there is only one excited state at about 514.4 nm for the PATP/Ag_5 complex and at about 632.8 nm for the PATP/Au_5 complex which are suitable for studying the resonance Raman effect via Albrecht's A term (the Frank–Condon term). We calculated the SERRS of the PATP/Au_5 complex at 633 nm. From Figure 3h, the profile of the pre-resonance Raman spectrum at the incident wavelength of 633 nm is similar to that of the normal Raman spectrum of the PATP/Au_5 complex (Figure 3e), and the intensity of Raman spectrum was enhanced by a factor on the order of 10^3. The experimental SERRS spectrum in ref. [26] is quite different from that calculated at an incident wavelength of 633 nm. Thus, the experimental SERRS spectrum does not exclusively contain contributions from the Frank–Condon term, and it is necessary to consider the Herzberg–Teller mechanism.

When the size of the metal cluster is increased in calculations, there are more excited electronic states for the metal/molecule complex.[13,14] For PATP/metal complexes, if more than one excited states are near the energy of the incident wavelength of the laser, and the product of the symmetry of both excited states is equal to or contains the b_2 symmetry, the b_2 modes in the PATP/metal complex will be strongly enhanced. We calculated the optical absorption spectrum of the PATP/Ag_{19} complex (fifty singlet excited states), which is shown in Figure 4. The excited-state properties of the complex PATP/Ag_{19} were investigated by means of charge difference density around 514 nm (514 ± 20 nm). Seven excited states were

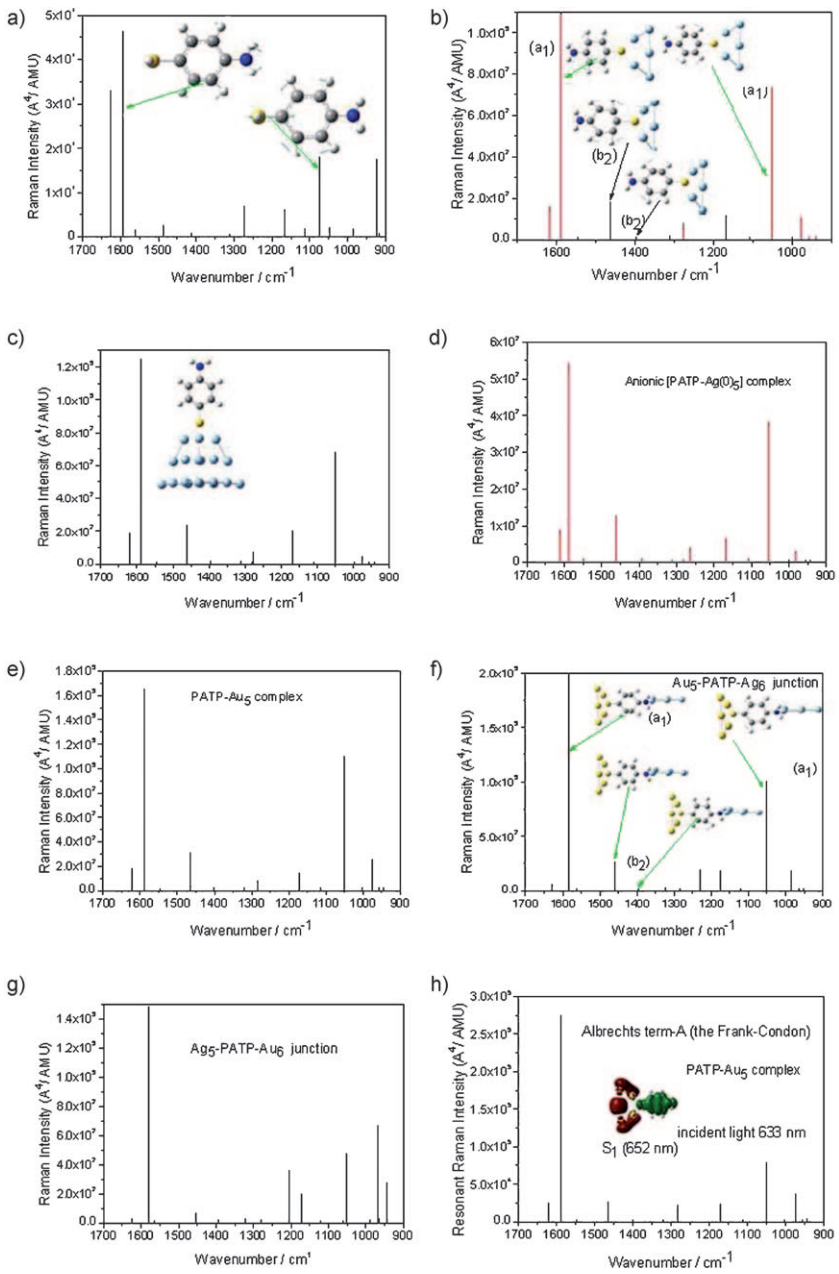

Figure 3. Calculated NRS spectra for a) PATP; b) PATP/Ag_5, c) PATP/Ag_{19}, d) anionic PATP/Ag_5, and e) PATP/Au_5 complexes; f) Au_5/PATP/Ag_6 junction; and g) Ag_5/PATP/Au_6 junction. h) SERRS of PATP/Au_5 complex excited at 632.8 nm. The scaling factor of the frequencies was set to 0.96 in our calculations for comparison with experimental results. The inset in h) is the charge difference density, and green and red stand for hole and electron, respectively.

found. According to the visualization of charge difference density in Figure 5, there are two kinds of excited properties: one is collective intracluster excitations (S_{19} and S_{24}, in which all the electron and hole are localized on the Ag_{19} cluster), which is direct evidence for electromagnetic mechanism; and the second is CT from PATP to the Ag_{19} cluster, which is direct evidence for the chemical mechanism via CT. Regarding the electromagnetic enhancement of the electronic transitions of S_{19} and S_{24}, even though the Ag_{19} cluster can not fully reflect the delocalized surface-plasmon modes (collective motions of the conduction electrons), Schatz et al. have successfully applied TDDFT to study the absorption and Raman scattering of Ag_{20}/pyridine[12a] and Ag_{20}/pyridazine/Ag_{20} model systems.[12b] Their results indicate that the absorption properties of a 20-atom tetrahedral silver cluster behave quite similarly to plasmon excitation observed in nanoparticles, and the Raman enhancement due to this cluster is comparable to findings on larger nanoparticles (>10 nm). For the electromagnetic mechanism, Raman peaks would not be selectively enhanced. For the strongly selective enhancements of b_2 modes in experiments, the contribution should be from chemical enhancement via CT. As discussed above (see Figure 3h), b_2 modes can not be strongly enhanced by the Frank–Condon term, so we focus on the coupling of CT excited states for the Herzberg–Teller mechanism.

Herzberg-Teller-surface selection rule is [Eq. (3)][39]

$$\Gamma(Q_K) = \sum_K \Gamma(\mu_{CT}) \times \Gamma_K \qquad (3)$$

where $\Gamma(Q_K)$ is the irreducible representation to which the allowed SERS vibration belongs, $\Gamma(\mu_{CT})$ the irreducible representation to which the component of the charge-transfer dipole perpendicular to the surface belongs (in the combined molecule/metal system), and Γ_K the irreducible representation of the molecular excited-state to which an optical transition is allowed.

According to the distribution of holes on PATP from charge difference densities for these CT excited states shown in Figure 5, there are two kinds of CT excited states. For S_{20}, the holes on PATP are only localized on the atoms, while for S_{18}, S_{21}, S_{22}, and S_{23}, the holes on PATP are not only localized on the atoms, but are also distributed over the bonds between C atoms (the symmetry of hole distribution on PATP is C_{2v}). For the molecule with C_{2v} symmetry,[39] $\Gamma(\mu_{CT})$ for these (S_{18}, S_{20}–S_{23}) excited states is A_1, according to the orientation of CT from PATP to metal cluster.

Now, we discuss Γ_K of PATP. Experimentally, three absorption bands of PATP were observed around 200, 250, and 300 nm,

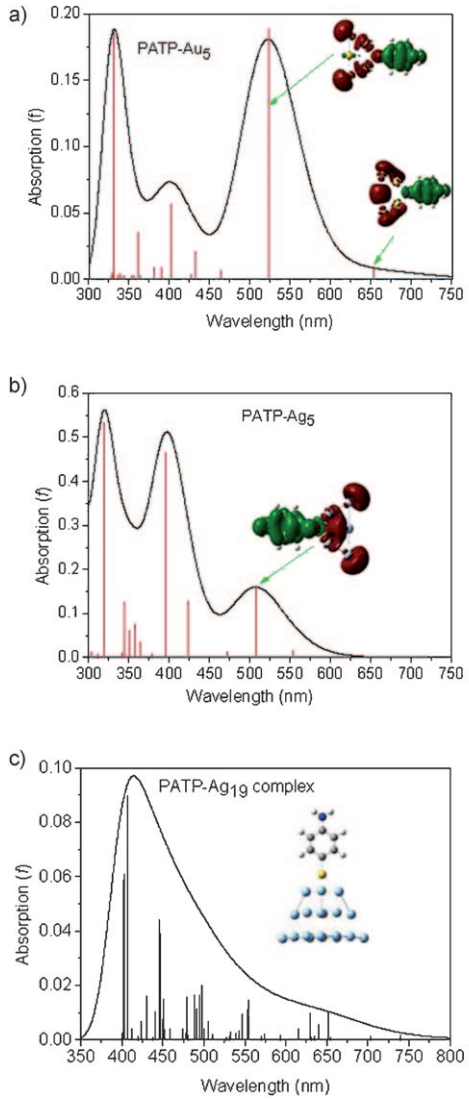

Figure 4. Calculated optical absorption spectra for a) PATP/Au_5, b) PATP/Ag_5, and c) PATP/Ag_{19}. The insets in a) and b) are charge difference densities, and green and red stand for hole and electron, respectively.

which are closely related to $B_{a,b}$, L_a, and L_b in Platt's notation.[18] The last two transitions are symmetry-forbidden, but the substituents on the benzene ring lower the symmetry and introduce some allowed character into the symmetry-forbidden transitions. The L_a and L_b transitions are x (a_1) and y (b_2), respectively. For substituted benzene the ν_{8b} mode (1579 cm^{-1}) can couple the L_a transition with the b component of the $B_{a,b}$ transition. On the other hand, the L_b transition is coupled to the $B_{a,b}$ transition via ν_{8a}, ν_{8b}, ν_{19a} and ν_{9a} modes. Osawa et al.[18] show that the appearance of strong lines of b_2 symmetry are due to intensity borrowing from an intense $\pi \rightarrow \pi^*$ molecular transition ($^1A_1 \rightarrow {}^1B_2$) at 200 nm.[18,39] Then, Equation (3) can be written as for (S_{18}, S_{20}–S_{23}) electronic transitions [Eq. (4)]

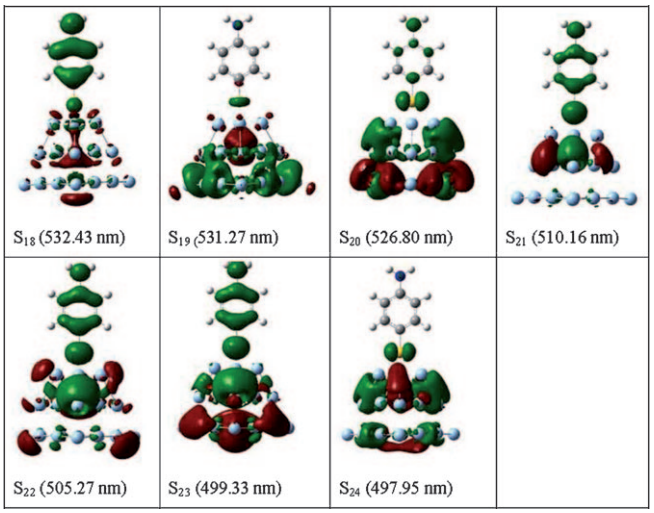

Figure 5. Charge difference densities from S_{18} to S_{24} near 514.4 nm for the PATP/Ag_{19} complex, where green and red stand for hole and electron, respectively.

$$\Gamma(Q_K) = A_1 \times (L_b + L_a + B_2) \approx A_1 \times B_2 \quad (4)$$

So, according to the Herzberg–Teller surface selection rules, the vibrations of the $b_2(A_1 \times B_2)$ mode are strongly enhanced in SERS by the Herzberg–Teller term via CT. Because of the heavy computational demand of the SERRS spectrum for such large system, the simulated SERRS spectrum was not calculated theoretically in this paper. Here we just point out the importance of the chemical mechanism in SERRS of the PATP/Ag_{19} complex due to charge transfer and the Herzberg–Teller mechanism.

2.3. Excited-State Properties and Chemical Mechanism in SERRS Spectra of Metal/Molecule/Metal Junctions

The calculated NRS spectrum of the Au_5/PATP/Ag_6 junction (Figure 3 g) is significantly different from the experimental SERS spectra of this sandwich structure in ref. [24]. The vibrations of totally symmetric a_1 modes at 1076 cm^{-1} and 1578 cm^{-1}, and nontotally symmetric b_2 modes at 1392 and 1439 cm^{-1} in the experimental Raman spectrum in ref. [24] are shown in the inset in Figure 3 f. Thus, the experimental SERS spectrum should not correspond to the NRS spectrum. We calculated the first two singlet excited states in optical absorption of the Au_5/PATP/Ag_6 junction with different functionals and the same basis set (see Table 2). When calculated with the B3LYP functional, S_1 lie at 989 nm, which is near the experimental incident wavelength of 1064 nm. Hence, the experimental SERS

Table 2. Calculated electronic transition energies and oscillator strengths f for Au_5/PATP/Ag_6 junction.

	TD-B3LYP/LANL2DZ				TD-B3PW91/LANL2DZ			
	eV	nm	f	CI coefficients	eV	nm	f	CI coefficients
S_1	1.2530	989.52	0.0011	0.70505 (H→L)	1.3154	942.53	0.0007	0.70511 (H→L)
S_2	1.3986	886.46	0.0000	0.70557 (H−1→L)	1.4704	843.17	0.0000	0.70553 (H−1→L)

spectrum should correspond to the pre-resonance Raman scattering spectrum. The S_1 level calculated with the B3PW91 functional is 948 nm. The calculated energy difference with different functionals (B3LYP and B3PW91) is about 0.06 eV, which indicates that the results calculated with the B3LPY functional for metal/PATP/metal junctions are reliable. Density functional theory is known to underestimate the excitation energies for long-range CT excited states in weakly interacting complexes due to incorrect asymptotic behavior of approximate exchange-correction functionals (i.e., the self-energy error[40]); thus, it is possible that the CT excitations will occur at higher energies. On the other hand, with increasing cluster size, the calculated lowest absorption peak would be redshifted to nearer to 1064 nm, according to the comparison of the absorption peaks of the PATP/Ag_5 and PATP/Ag_{19} complexes. Furthermore, Schatz et al. successfully calculated the optical absorption spectra of the Ag_{20}/pyridine[12a] and Ag_{20}/pyridazine/Ag_{20}[12b] and rhodamine 6G (R6G)/Ag_2[41] model systems by the TDDFT method. The CT transition at 1010 nm for the R6G/Ag_2 model system was also obtained theoretically.[41] Thus, the experimental SERS spectra should be at least a case of a pre-resonance SERRS spectrum according to our calculations. There are two ways to test our calculated results. The first one is with the experimental electron energy loss (EELS),[42] and the second with long-range-corrected TDDFT.[40,43]

As the discussion on the b_2 vibrational modes in metal/PATP complex showed, the experimental SERRS of the Au_5/PATP/Ag_6 junction at an incident wavelength of 1064 in ref. [24] should have contributions from both the Frank–Condon and the Herzberg–Teller mechanisms. To confirm the contribution of the Herzberg–Teller mechanism, we investigated the S_1 and S_2 excited-state properties of the Au_5/PATP/Ag_6 junction by means of charge difference density. According to the charge difference density in Figure 6a, these two excited states are the charge-transfer excited states, in which electrons transfer directly by tunneling from the Au_5 cluster to the Ag_6 cluster instead of passing through PATP (this is also called intervalence charge transfer). Although the distributions of electrons on the Au_5 cluster are almost the same for these two excited states, the distribution of holes on the Ag_6 cluster is significantly different. The symmetries of tunneling CT from Ag_6 cluster to Au_5 cluster are different, the product of the different CT symmetries of these lowest singlet excited states should contain the b_2 symmetry, and the SERRS spectrum in experiment in ref. [24] must result from the Herzberg–Teller mechanism.

To interpret the electron tunneling transfer from the Ag_6 cluster to the Au_5 cluster on electronic excited states near 1064 nm, we checked the orbital energy levels of PATP/Au_5 complex and Ag_6 cluster (see Figure 6b) and the distributions of partial density of state (PDOS)[44] on these molecular orbitals (see Figure 6c). In the calculations, the geometries were those of the optimized Au_5/PATP/Ag_6 junction without further optimization. According to Figure 6b, the energy levels of HOMO and HOMO−1 for the Ag_6 cluster are located between those of the HOMO and LUMO of the PATP/Au_5 complex; while the energy level of the LUMO for the Ag_6 cluster is higher than that of PATP/Au_5 complex. Thus, the lowest electronic transition for the Au_5/PATP/Ag_6 junction should be from the HOMO and HOMO−1 of Ag_6 to the LUMO of the PATP/Au_5 complex, and the transition energy of the Au_5/PATP/Ag_6 junction is much lower (redshifted) than that of the Au_5/PATP complex (orbital transition from HOMO to LUMO for the Au_5/PATP complex). Furthermore, the PDOS of the LUMO for the PATP/Au_5 complex is localized on the Au_5 cluster (see Figure 6c), so electrons should transfer by tunneling from Ag_6 to Au_5 in the lowest electronic transition for the Au_5/PATP/Ag_6 junction.

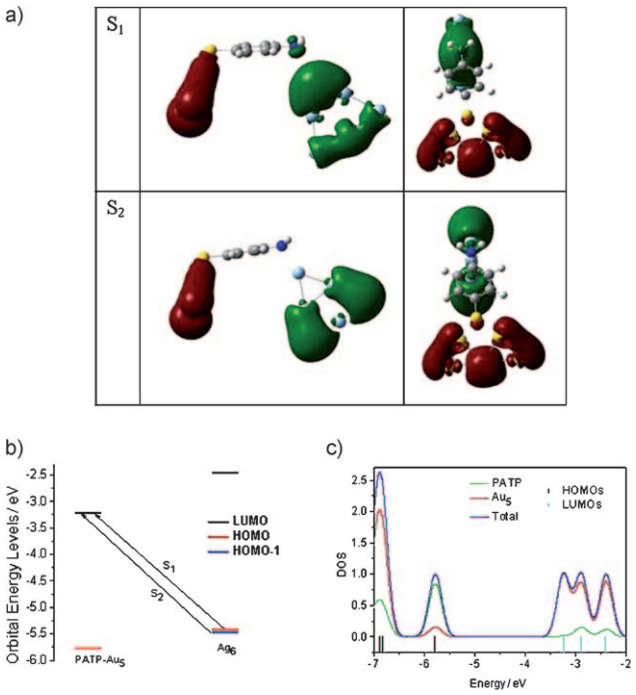

Figure 6. a) Charge difference densities from S_1 to S_2 near 1064 nm for the Au_5/PATP/Ag_6 junction, where green and red stand for hole and the electron, respectively. b) Orbital energies of PATP/Au_5 complex and Ag_6 cluster. c) Distribution of partial density of states (PDOS) for PATP/Au_5 complex, where the full width at half-maximum (FWHM) is set to 0.3 eV.

For the Ag_6 cluster, we assume that the Fermi energy level is located somewhere between the energy levels of the HOMO and LUMO in the case of the PATP/Au_5 complex [the simplest assumption is $E_{Fermi} = \frac{1}{2}(E_{HOMO} + E_{LUMO})$]. If the electrons are transferred from Fermi energy level or HOMO (or HOMO−1) of theAg_6 cluster to the LUMO energy level of PATP/Au_5 on electronic transition, optical absorption of the Au_5/PATP/Ag_6 junction at 1064 nm could occur, since the range of transition energy is from 1720 nm [electron transfer from the Fermi energy level of the Ag_6 cluster to the LUMO energy level of PATP/Au_5 on electronic transition, and assuming $E_{Fermi} = \frac{1}{2}(E_{HOMO} + E_{LUMO})$] to 836 nm (electron transfer from the HOMO of the Ag_6 cluster to the LUMO energy level of PATP/Au_5 on electronic transition). The lowest transition energy (ca. 989 nm) calculated with TDDFT/B3LYP-LANL2DZ method (Table 2) is within this range. Furthermore, because of the different CT symmetry of the intervalence charge transfer in the first two electronic excited states, the experimental SERS spectrum should be a SERRS spectrum, with contribution from the

Herzberg–Teller mechanism via electron tunneling transfer from the Ag_6 cluster to the Au_5 cluster.

When the nanoparticles were assembled inversely (with the silver nanoparticles as the first layer and the gold nanoparticles as the second in the experiment in ref. [24]), the b_2 modes of the interconnecting PATP molecules were not enhanced at an incident wavelength of 1064 nm. To interpret such a phenomenon, the NRS spectrum and excited state properties of the Ag_5/PATP/Au_6 junction were calculated. The calculated NRS spectrum (Figure 3g) is similar to the experimental SERS spectra of the Ag/PATP/Au sandwich structure in ref. [24]. Thus, the experimental SERS spectrum may be the NRS spectrum, and the enhancement may result from the static chemical enhancement via static CT at the ground state, due to the interactions between PATP and Ag and Au nanoparticles.

To further confirm this, we calculated the first singlet excited state in the optical absorption of the Ag_5/PATP/Au_6 junction with different functionals and the same basis set (see Table 3).

Table 3. Calculated electronic transition energies and oscillator strengths *f* for Ag_5/PATP/Au_6 junction.

	TD-B3LYP/LANL2DZ			TD-B3PW91/LANL2DZ		
	eV	nm	*f*	eV	nm	*f*
S_1	2.5275	490.54	0.0025	2.5909	478.54	0.0028

We found that the S_1 level calculated with the B3LYP functional is 490 nm, which is far from the experimental incident wavelength of 1064 nm. Hence, the experimental SERS spectrum at an incident wavelength of 1064 nm must be the NRS spectrum. The S_1 level calculated with B3PW91 functional is 478 nm. The calculated energy difference with different functionals (B3LYP and B3PW91) of about 0.06 eV indicates that the result calculated with the B3LPY functional for the metal/PATP/metal junction is reliable. From the charge difference density in Figure 7a, S_1 is the CT excited state, whereby electrons transfer from PATP to the Au_6 cluster.

To further answer the question why there is no optical absorption near 1064 nm, the molecular orbital energy levels of PATP/Ag_5 complex and Au_6 cluster were compared (see Figure 7b). In the calculations, the geometries are those of the optimized Ag_5/PATP/Au_6 junction without further optimization. From Figure 7b, we can see that the HOMO energy level of the PATP-Ag_5 complex is higher than that of the Au_6 cluster; and the LUMO energy level of the Au_6 cluster is lower than that of the PATP/Ag_5 complex. Hence, the lowest transition should be from the HOMO of the PATP/Ag_5 complex to the LUMO of the Au_6 cluster. Furthermore, the PDOS of the HOMO of the PATP/Ag_5 complex is localized on PATP (see Figure 7c), so CT should take place from PATP to the Au_6 cluster at the lowest transition energy. If electrons transfer from the HOMO of PATP/Ag_5 to the LUMO of Au_6 on electronic transition, the transition energy is about 2.53 eV (490 nm), and even if the electrons transfer from the HOMO of PATP/Ag_5 to the Fermi energy level of the Au_6 cluster on electronic transition, the transition energy would still about 1.82 eV (681 nm), assuming $E_{Fermi} = \frac{1}{2}(E_{HOMO} + E_{LUMO})$. Therefore, the calculated transitions are all above the incident wavelength of 1064 nm. The lowest transition energy (490 nm) calculated with the TDDFT/B3LYP-LANL2DZ method (Table 3) is almost the same as the energy of the orbital transition from the HOMO of PATP/Ag_5 to the LUMO of Au_6 on electronic transition.

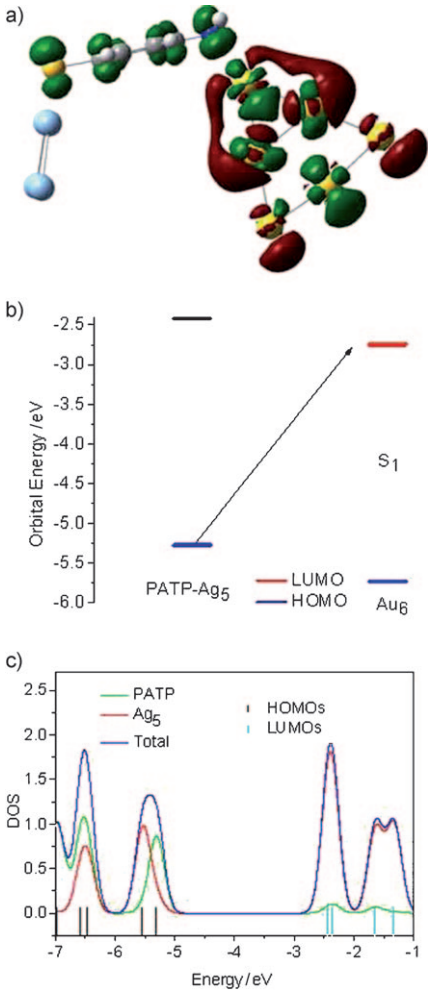

Figure 7. a) Charge difference density for S_1 of the Ag_5/PATP/Au_6 junction, where green and red stand for hole and electron, respectively. b) Orbital energies of PATP/Ag_5 complex and Au_6 cluster. c) Distribution of partial density of states (PDOS) for PATP/Ag_5 complex, where the FWHM is set to 0.3 eV.

3. Conclusions

We have investigated the chemical enhancement of the SERRS of the PATP molecule adsorbed on gold nanoparticles or silver nanoparticles and in metal/PAPT/metal junctions. We visualized intracluster and CT excitations by means of charge difference density, which provides visual evidence for the electromagnetic and chemical enhancements. The selective enhancements of the b_2 modes in SERS experiments should be due to the Herzberg–Teller mechanism via CT for metal/PATP complexes. For the Au_5/PATP/Ag_6 junction, the selective enhancement of b_2 modes at an incident wavelength of 1064 nm in the experi-

mental SERRS spectrum should be due to the Herzberg–Teller mechanism via electron tunneling transfer from the Ag_6 cluster to the Au_5 cluster. For the Ag_5/PATP/Au_6 junction, the b_2 modes are not selectively enhanced at an incident wavelength of 1064 nm in the experimental SERS spectrum, which is the NRS spectrum.

Acknowledgements

This work was supported by the National Natural Science Foundation of China (Grant Nos. 10874234, 10874233, 20703064, and 10625418), Sino-Swedish Collaborations about Nanophotonics and Nanoelectronics (2006DFB02020), National Basic Research Project of China (Grant Nos. 2009CB930701 and 2007CB936804), and "Bairen" projects of CAS.

Keywords: charge transfer · density functional calculations · Raman spectroscopy · surface-enhanced resonance

[1] M. Fleischmann, P. J. Hendra, A. J. McQuillan, *Chem. Phys. Lett.* **1974**, *26*, 163–166.
[2] D. L. Jeanmaire, R. P. Van Duyne, *J. Electroanal. Chem. Inferfacial Electrochem.* **1977**, *84*, 1–20.
[3] M. G. Albrecht, J. A. Creighton, *J. Am. Chem. Soc.* **1977**, *99*, 5215–5217.
[4] M. Moskovits, *Rev. Mod. Phys.* **1985**, *57*, 783–826.
[5] K. Kneipp, H. Kneipp, I. Itzkan, R. R. Dasari, M. S. Feld, *Chem. Rev.* **1999**, *99*, 2957–2976.
[6] H. X. Xu, E. J. Bjerneld, M. Kail, L. Borjesson, *Phys. Rev. Lett.* **1999**, *83*, 4357–4360.
[7] H. X. Xu, M. Kall, *Phys. Rev. Lett.* **2002**, *89*, 246802.
[8] H. Metiu, P. Dos, *Annu. Rev. Phys. Chem.* **1984**, *35*, 507–536.
[9] A. Otto, I. Mrozek, H. Grabhorn, W. Akemann, *J. Phys. Condens. Matter* **1992**, *4*, 1143–1212.
[10] a) A. C. Albrecht, *J. Chem. Phys.* **1961**, *34*, 1476–1484; b) J. R. Lombardi, R. L. Birke, T. Lu, J. Xu, *J. Chem. Phys.* **1986**, *84*, 4174–4180.
[11] D. Y. Wu, X. M. Liu, S. Duan, X. Xu, B. Ren, S. H. Lin, Z. Q. Tian, *J. Phys. Chem. C* **2008**, *112*, 4195–4204.
[12] a) L. L. Zhao, L. Jensen, G. C. Schatz, *J. Am. Chem. Soc.* **2006**, *128*, 2911–2919; b) L. L. Zhao, L. Jensen, G. C. Schatz, *Nano Lett.* **2006**, *6*, 1229–1234.
[13] M. T. Sun, S. B. Wan, Y. J. Liu, Y. Jia, H. X. Xu, *J. Raman Spectrosc.* **2008**, *39*, 402–408.
[14] M. T. Sun, S. S. Liu, M. D. Chen, H. X. Xu, *J. Raman Spectrosc.*, DOI: 10.1002/jrs.2093.
[15] F. J. Adrian, *J. Chem. Phys.* **1982**, *77*, 5302–5314.
[16] A. Campion, P. Kambhampati, *Chem. Soc. Rev.* **1998**, *27*, 241–250.
[17] W. Hill, B. Wehling, *J. Phys. Chem.* **1993**, *97*, 9451–9455.
[18] M. Osawa, N. Matsuda, K. Yoshii, I. Uchida, *J. Phys. Chem.* **1994**, *98*, 12702–12707.
[19] J. Wang, T. Zhu, Z. F. Liu, *Acta Phys. -Chim. Sin* **1998**, *14*, 485–489.
[20] L. Cao, P. Diao, L. Tong, T. Zhu, Z. F. Liu, *ChemPhysChem* **2005**, *6*, 913–918.
[21] J. W. Gibson, B. R. Johnson, *J. Chem. Phys.* **2006**, *124*, 064701.
[22] D. P. Fromm, A. Sundaramurthy, A. Kinkhabwala, P. J. Schuck, G. S. Kino, W. E. Moerner, *J. Chem. Phys.* **2006**, *124*, 061101.
[23] M. Baia, F. Toderas, L. Baia, J. Popp, S. Astilean, *Chem. Phys. Lett.* **2006**, *422*, 127–132.
[24] Q. Zhou, X. W. Li, Q. Fan, X. X. Zhang, J. W. Zheng, *Angew. Chem.* **2006**, *118*, 4074–4077; *Angew. Chem. Int. Ed.* **2006**, *45*, 3970–3973.
[25] Q. Zhou, G. Zhao, Y W. Chao, Y. Li, Y. Wu, J. W. Zheng, *J. Phys. Chem. C* **2007**, *111*, 1951–1956.
[26] F. Toderas, M. Baia, L. Baia, S. Astilean, *Nanotechnology* **2007**, *18*, 255702.
[27] Y. L. Wang, X. Q. Zou, W. Ren, W. D. Wang, E. K. Wang, *J. Phys. Chem. C* **2007**, *111*, 3259–3270.
[28] Q. Zhou, Y. W. Chao, Y. Li, W. Wu, Y. Wu, J W. Zheng, *ChemPhysChem* **2007**, *8*, 921–925.
[29] P. Hohenberg, W. Kohn, *Phys. Rev.* **1964**, *136*, B864–B687.
[30] A. D. Becke, *Phys. Rev. A* **1988**, *38*, 3098–3100.
[31] J. P. Perdew, *Phys. Rev. B* **1986**, *33*, 8822–8824.
[32] K. T. Carron, L. G. Hurley, *J. Phys. Chem.* **1991**, *95*, 9979–9984.
[33] P. J. Hay, W. R. Wadt, *J. Chem. Phys.* **1985**, *82*, 270–283.
[34] E. K. U. Gross, W. Kohn, *Phys. Rev. Lett.* **1985**, *55*, 2850–2852.
[35] There is an imaginary frequency of magnitude of 4.63 cm^{-1}, which is most likely due to a small inaccuracy in the numerical grid.
[36] Gaussian 03 (Revision E.01), M. J. Frisch, G. W. Trucks, H. B. Schlegel, G. E. Scuseria, M. A. Robb, J. R. Cheeseman, J. A. Montgomery, Jr., T. Vreven, K. N. Kudin, J. C. Burant, J. M. Millam, S. S. Iyengar, J. Tomasi, V. Barone, B. Mennucci, M. Cossi, G. Scalmani, N. Rega, G. A. Petersson, H. Nakatsuji, M. Hada, M. Ehara, K. Toyota, R. Fukuda, J. Hasegawa, M. Ishida, T. Nakajima, Y. Honda, O. Kitao, H. Nakai, M. Klene, X. Li, J. E. Knox, H. P. Hratchian, J. B. Cross, C. Adamo, J. Jaramillo, R. Gomperts, R. E. Stratmann, O. Yazyev, A. J. Austin, R. Cammi, C. Pomelli, J. W. Ochterski, P. Y. Ayala, K. Morokuma, G. A. Voth, P. Salvador, J. J. Dannenberg, V. G. Zakrzewski, S. Dapprich, A. D. Daniels, M. C. Strain, O. Farkas, D. K. Malick, A. D. Rabuck, K. Raghavachari, J. B. Foresman, J. V. Ortiz, Q. Cui, A. G. Baboul, S. Clifford, J. Cioslowski, B. B. Stefanov, G. Liu, A. Liashenko, P. Piskorz, I. Komaromi, R. L. Martin, D. J. Fox, T. Keith, M. A. Al-Laham, C. Y. Peng, A. Nanayakkara, M. Challacombe, P. M. W. Gill, B. Johnson, W. Chen, M. W. Wong, C. Gonzalez, J. A. Pople, Gaussian, Inc., Pittsburgh, PA, **2004**.
[37] J. Neugebauer, M. Reiher, C. Kind, B. A. Hess, *J. Comput. Chem.* **2002**, *23*, 895–910.
[38] J. B. Foresman, E. Frisch, *Exploring Chemistry with Electronic Structure Methods*, 2nd ed., Gaussian, Pittsburgh, **2004**.
[39] J. R. Lombardi, R. L. Birke, *J. Phys. Chem. C* **2008**, *112*, 5605–5617.
[40] A. Dreuw, M. Head-Gordon, *J. Am. Chem. Soc.* **2004**, *126*, 4007–4016.
[41] J. Zhao, L. Jensen, J. Sung, S. Zou, G. C. Schatz, R. P. Van Dunyne, *J. Am. Chem. Soc.* **2007**, *129*, 7647–7656.
[42] P. Avouris, J. E. Demuth, *J. Chem. Phys.* **1981**, *75*, 4783–4794.
[43] Y. Tawada, T. Tsuneda, S. Yanagisawa, T. Yanai, K. Hirao, *J. Chem. Phys.* **2004**, *120*, 8425–8433.
[44] N. O'Boyle, *GaussSum*, Revision 2.1., http://GaussSum.sf.net.

Received: September 9, 2008
Revised: November 4, 2008
Published online on December 12, 2008

